

The effect of welding conditions on solidification cracking susceptibility of type 310S stainless steel during laser welding using an in-situ observation technique

Kota Kadoi · Akira Fujinaga · Motomichi Yamamoto · Kenji Shinozaki

Received: 3 October 2012 / Accepted: 13 January 2013 / Published online: 14 March 2013
© The Author(s) 2013. This article is published with open access at Springerlink.com

Abstract Solidification cracking occurs easily at high welding speeds, and should therefore occur more easily during laser welding. Both the solidification behavior and thermal strain change depend on the welding speed, and therefore, the critical strain for solidification cracking must be measured to clarify the factors influencing the solidification cracking susceptibility. However, the critical strain required for solidification cracking under high welding speed conditions has not yet been determined. The aim of this work was to investigate the effect of welding speed on the solidification cracking susceptibility of Type 310S stainless steel. U-type hot cracking tests were conducted using a developed in-situ observation technique with high-speed camera, and the critical strain for solidification cracking was evaluated quantitatively. The critical strain for solidification crack initiation decreased with increasing welding speed. The distribution of residual liquid depended on the microstructure, and the morphological distribution of the residual liquid changed from a droplet to a thin film with increasing welding speed. The transition in distribution morphology of the residual liquid implies the material is susceptible to solidification cracking.

Keywords (IIW-Thesaurus) Hot cracking · Solidification cracking · Laser welding

1 Introduction

A technique to prevent solidification cracking is required in the welding process, because stainless steels, nickel-based superalloys and dissimilar welded joints are susceptible to this phenomenon. Solidification cracking becomes a more serious problem when different materials and an increased welding speed are used for the high functionalization of the mechanical structure and to increase productivity [1]. Optimization of the welding joint design and development of the welding material have been attempted to prevent the occurrence of solidification cracks. However, a definite prevention technique for solidification cracking has not yet been developed. Thus, it is necessary to investigate both the solidification phenomenon and distribution of loaded strain during welding in detail, and to elucidate the mechanism of the solidification cracking phenomenon.

It is well known that solidification cracking occurs between the liquidus and solidus temperatures by the strain loaded on the residual liquid from solidification shrinkage and constraint forces. The critical strain for initiating cracks is affected by factors such as the solidification morphology, corresponding to chemical composition, segregation of sulfur and phosphorus, strain rate, welding condition and so on [1–5]. To date, the solidification cracking susceptibility has been evaluated using a high temperature ductility curve, which is the relationship between the critical strain and temperature for solidification crack initiation. Thus, the critical strains and solidification crack initiation temperature must be measured quantitatively and precisely to understand in detail the solidification cracking phenomenon.

Laser welding is an attractive welding processes, and is expected to increase in practical use because of its high

Doc. IIW-2341, recommended for publication by Commission IX
“Behaviour of Metals Subjected to Welding.”

K. Kadoi (✉) · A. Fujinaga · M. Yamamoto · K. Shinozaki
Graduate School of Engineering, Hiroshima University,
1-4-1 Kagamiyama, Higashi-Hiroshima,
Hiroshima 739-8527, Japan
e-mail: kadoi@hiroshima-u.ac.jp

welding speed, low deformation and so on. Since the solidification behavior and thermal strain are dependent on welding speed, an increase in welding speed should cause materials to be more susceptible to solidification cracking [1, 2, 6–8]. However, no one has determined the critical strain for solidification cracking under high welding speed conditions.

In this paper, we study the effect of welding speed on the solidification cracking susceptibility of Type 310S stainless steel, which is susceptible to solidification cracking at high welding speeds. This steel also enabled the evaluation of microstructure at room temperature, because of its advantage in solidifying the single austenite phase without transformation. It is necessary to measure accurately both the strain and temperature for crack initiation during rapid cooling at high temperature, to elucidate the solidification cracking phenomenon at high welding speed conditions. An in-situ observation technique using a high-speed camera developed by us [9, 10], was used to measure the strain history during U-type hot cracking tests. In addition, an optical fiber radiation thermometer was used with higher response rate than thermocouples used for the measurement of temperature history during welding.

2 Experimental procedure

Type 310S stainless steel with chemical composition in Table 1 was used as the test specimen. The specimen thickness was 2 mm, with width of 50 mm and length of 110 mm. Figure 1 shows the experimental setup of the U-type hot cracking test with vertical in-situ observation system using a high-speed camera. The welding conditions are shown in Table 2. Fiber laser (IPG, YLR-300-S) was used as a heat source. To investigate the influence of welding speed on the solidification cracking susceptibility, the welding speed was varied from 0.4 to 1.6 m/min. The laser spot size was 0.4 mm and the laser power was adjusted to obtain full penetration beads in each welding speed. The laser head was tilted 30° to the welding direction to prevent interference with the camera setup. The high-speed camera was set up with a zoom lens attached with a hot mirror for highly magnified observation and monitoring of a visible ray only. A metal halide lamp was also used as a lighting system to obtain clear images. Ar gas was blown onto the surface and rear of the specimen to prevent oxidation during laser welding.

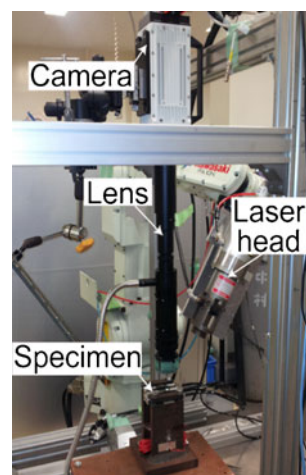


Fig. 1 Experimental setup of vertical in-situ observation method

Hot cracking tests require the reproduction of solidification cracks and measurement of the local critical strain for crack initiation. In this study, we carried out U-type hot cracking tests with in-situ observations using the high-speed camera set up. A U-type cracking tester can generate solidification cracks at the center line of the weld bead by applying a vertical load to the welding direction.

The sequence of the U-type hot cracking test is as follows. First, the restraint beams were bent to a certain experimental distance by an external load. Then the specimen was fixed between the beam chucking plates. The initial tensile load was applied to the specimen after release of the external load. The transverse tensile load stretched the specimen and led to the generation of solidification cracks during welding. The edge of the molten pool was monitored continuously during laser welding by high-speed camera to observe the solidification sequences (crack initiation). Figure 2 shows a typical example of an image obtained by in-situ observation. Solidification cracks can be observed at the rear of the molten pool edge (Fig. 2a). The critical strain was measured from the videos by image analysis. As shown in Fig. 2b, when a solidification crack was found to have been initiated, two reference points, which were dendrite tips and/or an unevenness on the solid surface near the crack, were chosen along the tensile direction. The time at which the crack initiation occurred was termed t_1 and the distance between the two reference points at t_1 was measured as L_1 . The reference points were traced by rewinding the video and the starting tensile strain loading

Table 1 Chemical composition of Type 310S stainless steel

Type 310S	C	Si	Mn	P	S	Ni	Cr	Fe
50 (l)×110(w)×2 mm(t)	0.05	0.70	0.81	0.022	0.0004	19.18	24.98	Bal.

Table 2 Welding conditions

Welding speed, m/min	0.4	0.8	1.6
Laser power, kW	1.5	1.8	3.0
Laser spot diameter, mm	0.4		
Shape of penetration	Full penetration		
Laser irradiation angle, deg	30		
Ar shielding gas, l/min	50 (topside) 15 (backside)		

time ($t = t_0$) was determined as the reference point when the molten pool edge forms by solidification. Then, the distance between the reference points at t_0 was measured as L_0 . Finally, the critical strain for crack initiation was calculated by dividing the distance change ($L_1 - L_0$) by the initial distance (L_0). The initial distance L_0 was 0.5 mm. The initial tensile load can be controlled by changing the bending distance between beams.

To plot a high temperature ductility curve, the time when the strain for solidification cracking initiation was measured had to be correlated with a temperature. In addition, high accuracy and response temperature measurements were required, because the cooling rates are fast at high welding speeds. An optical fiber radiation thermometer with higher response rate than that of the thermocouples was used, and the temperature history during laser welding was measured by inserting it at the rear of the molten pool.

Optical microscope and scanning electron microscope were used to evaluate the fracture surfaces and microstructures of the weld bead. High resolution in-situ observations were also carried out to observe the distribution of the residual liquid at the rear of the molten pool during solidification.

3 Results and discussion

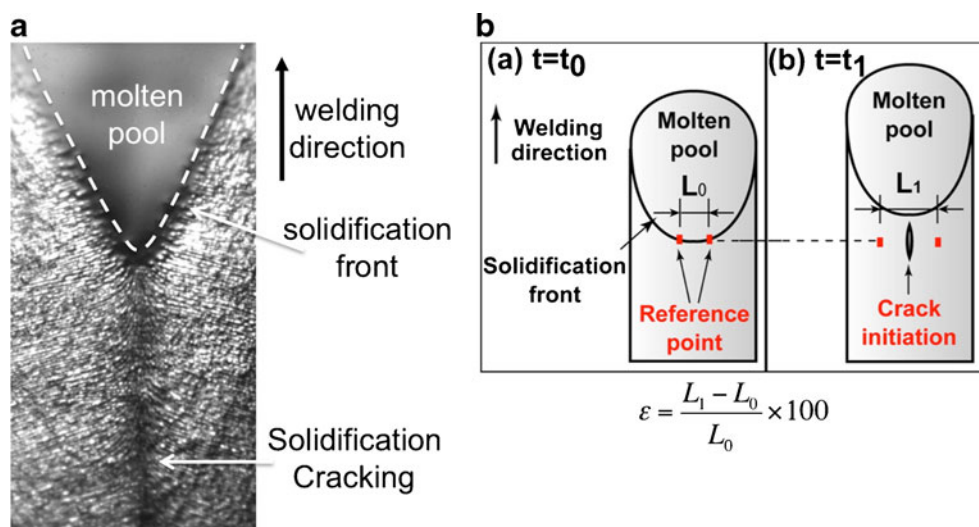
3.1 High temperature ductility curve

Figure 3 shows the strain histories at each welding speed obtained by U-type hot cracking tests. Initiations of solidification cracking were observed at the rear of the molten pool at every welding speed. The change in strain value during welding can be measured quantitatively up to crack initiation. The strain values of crack initiation were measured at a shorter time with increasing welding speed. In addition, the values obtained at 0.4 m/min were much higher than the values at other welding speeds and the minimum strain for crack initiation at 0.4 m/min was approximately 3 %.

The temperature histories of the molten pool at each welding speed are shown in Fig. 4. By using an optical fiber radiation thermometer, the temperature history can be measured with a high degree of accuracy, even though the cooling rate is quite high at a welding speed of 1.6 m/min. The cooling rate at 1.6 m/min is approximately 750 °C/s. The liquidus temperatures were determined by differentiating the cooling curves and the temperatures at 0.4, 0.8 and 1.6 m/min were 1406, 1408 and 1407 °C, respectively. This indicates that the influence of cooling rate on the liquidus temperature is insignificant.

Figure 5 shows the high temperature ductility curves at each welding speed. The horizontal axis is converted from time to temperature using the temperature history (Fig. 4), and the curve is obtained by connecting the critical strains for crack initiation. The tendencies of the strain change with temperature at 0.8 and 1.6 m/min are nearly the same. On the other hand, the strain values obtained at 0.4 m/min are much larger than those at the other welding speeds. Therefore, an increase in welding

Fig. 2 Schematic illustrations of measurement method for critical strain of solidification cracking **a** Images obtained by in-situ observation **b** Measurement method for critical strain



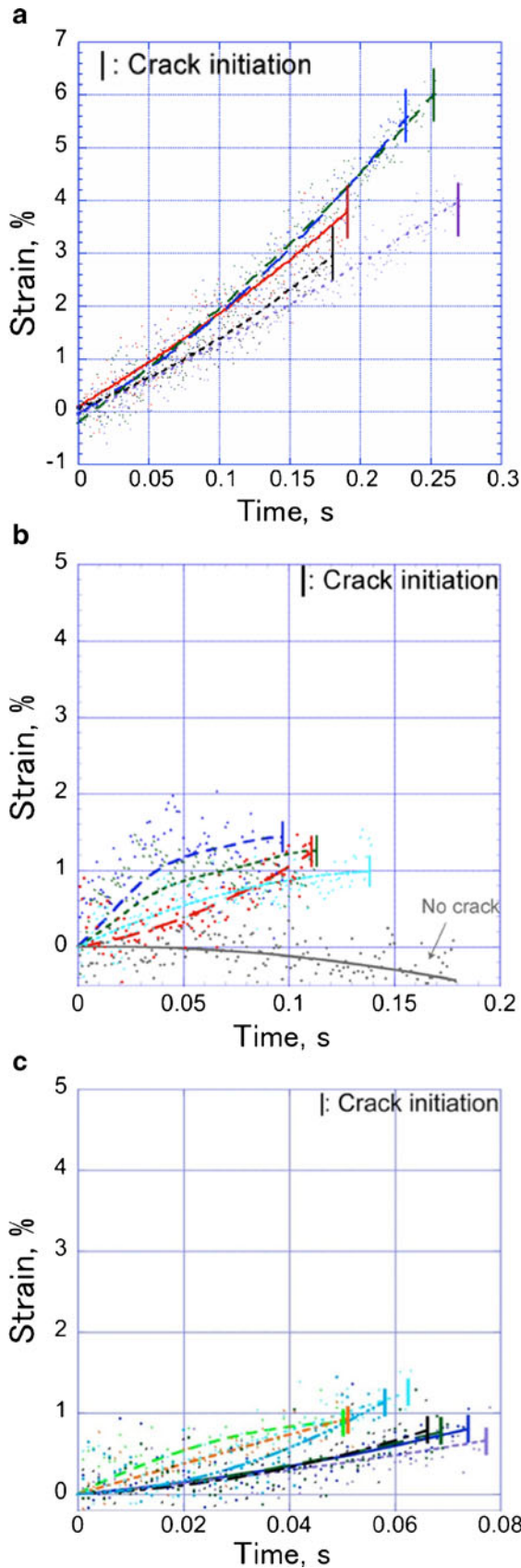


Fig. 3 Strain history during welding at various welding speeds **a** 0.4 m/min **b** 0.8 m/min **c** 1.6 m/min

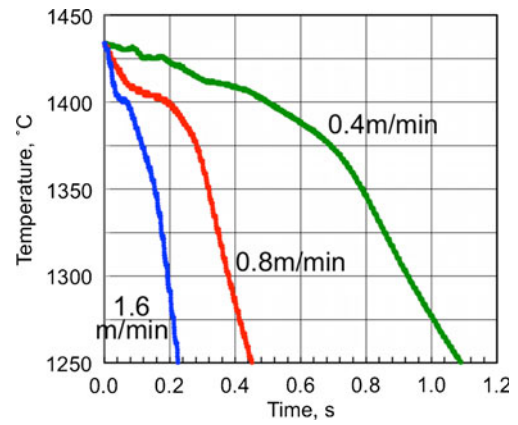


Fig. 4 Temperature history measured by optical fiber radiation thermometer

speed causes a decrease in solidification cracking susceptibility.

3.2 Microstructure of weld bead and fracture surface

Microstructures of the weld bead surface obtained at various welding speeds are shown in Fig. 6. The growth direction of the columnar dendrite varies from an incline to a direction perpendicular to the welding direction with welding speed. The angle of the direction of growth to the welding direction at 0.4, 0.8 and 1.6 m/min is 79.0, 84.1 and 86.6°, respectively. The dendrite size decreases with increase in welding speed. This may be caused by the increase in cooling rate corresponding to the welding

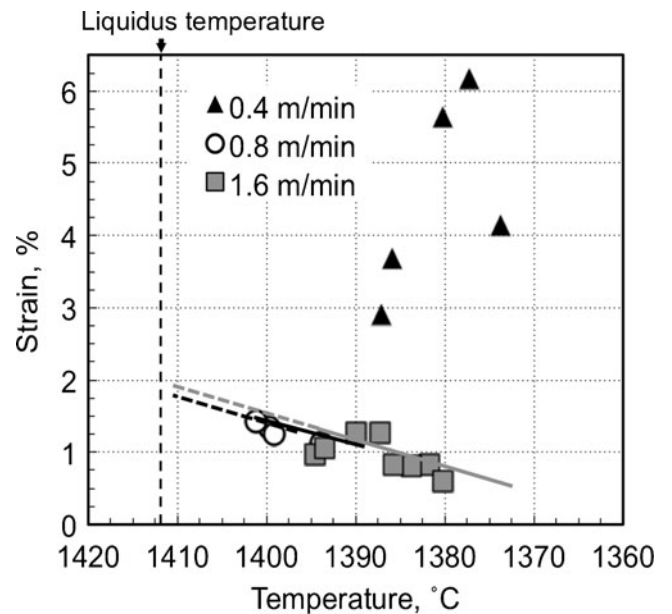


Fig. 5 High temperature ductility curves (specimens were welded under various welding speeds)

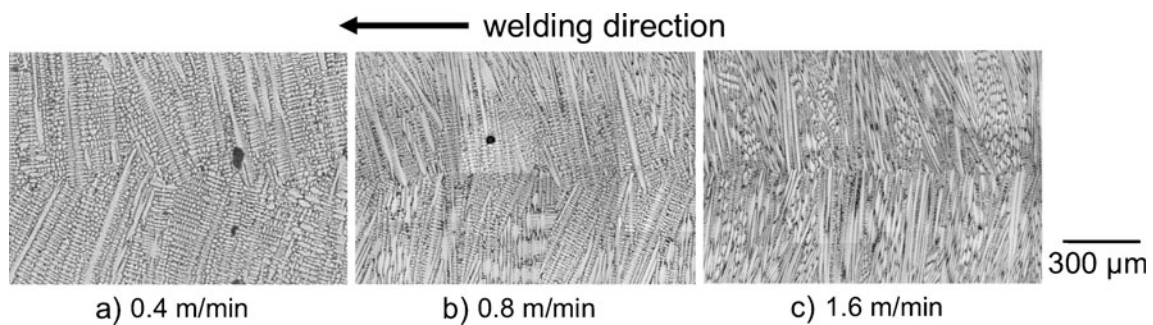


Fig. 6 Microstructures of weld bead center of samples welded under various welding speeds **a** 0.4 m/min **b** 0.8 m/min **c** 1.6 m/min

speed. The unevenness of the interface between the dendrite tips also increases with decreasing welding speed. Cross sections of the weld beads revealed that the columnar dendrites grow in the direction of the center of the weld bead at every weld speed.

Figure 7 shows fracture surfaces at the point of cracking generation at various welding speeds. Solidification cracks can be generated at all welding speeds because dendritic crystals are found at all welding conditions. There is no significant difference between crystal morphologies, and the crystals grow perpendicularly to the welding direction. The dendritic crystal size decreases with increasing welding speed.

3.3 High resolution in-situ observation

Figure 8 indicates the sequence at the rear of the molten pool during welding at 1.6 m/min, obtained by high resolution in-situ observations.

The molten pool is present in the long region along the center line of the welding bead initially ($t=0$, s) and the width of the molten pool becomes narrow at 0.04 s. After 0.08 s, solid phases start to form within the molten pool. The amount of solid increases with time, and the columnar grains grow perpendicularly to the welding direction bridge, with the solid growing from the opposite side at the bead center at 0.09 s. At 0.1 s, the liquid continues to remain between the columnar

grains, even though the amount of liquid is reduced significantly. Finally ($t=0.12$ s), the residual liquid exists as a droplet along the boundary between the columnar grain tips (bead center). High resolution in-situ observations reveal the sequences in solidification and distribution of residual liquid during laser welding. The columnar grains tend to bridge at the center of the weld bead and the liquid remains at the interface of the grain tips after bridging.

Figure 9 compares images between the high resolution in-situ observation and microstructure of the weld bead surface. A great amount of residual liquid is observed in the area between the broken lines in Fig. 9a. This area corresponds to the area in which dendrite arms are found as shown in Fig. 9b. Therefore, the liquid still remains at the center of the weld bead after bridging, and transforms into dendrite arms (solid).

3.4 Effect of welding speed on solidification cracking susceptibility

The distribution and amount of liquid phase at the terminal stages of solidification have been known to affect the solidification cracking susceptibility. The discussion of susceptibility focuses on the liquid distribution at a boundary between the columnar grains growing in an identical direction [2–5]. The presence of the liquid at the boundary in a wide temperature range (which exists

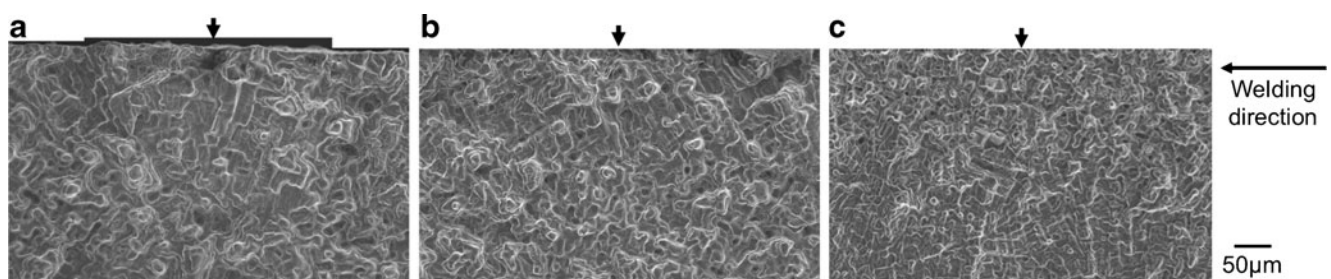


Fig. 7 Fracture surfaces generated at weld bead centers. Arrows indicate the point of crack generation **a** 0.4 m/min (1377 °C, 1.36 %) **b** 0.8 m/min (1393 °C, 1.12 %) **c** 1.6 m/min (1380 °C, 0.6 %)

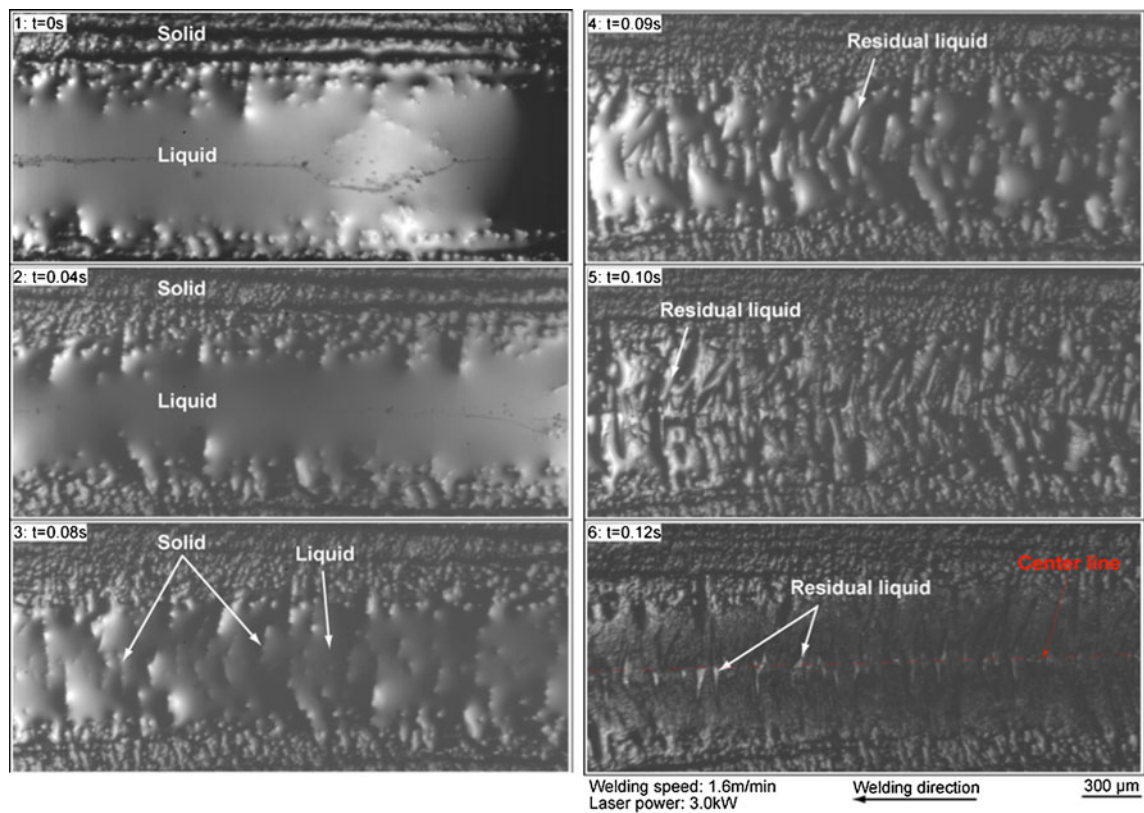


Fig. 8 Solidification sequence obtained by high magnified in-situ observation technique (welding speed: 1.6 m/min)

like a film) causes the material to be susceptible to solidification cracking.

In this study, solidification cracks were generated at the rear of the molten pool. Columnar grains grew perpendicularly to the welding direction and bridged the columnar grains growing from the opposite side at the rear. The liquid still remains at the interface of the grain tips after bridging, as indicated in Figs 8 and 9. In addition, the length of the liquid phase distribution at the center of the weld bead to the welding direction increases with increasing welding speed. This should be

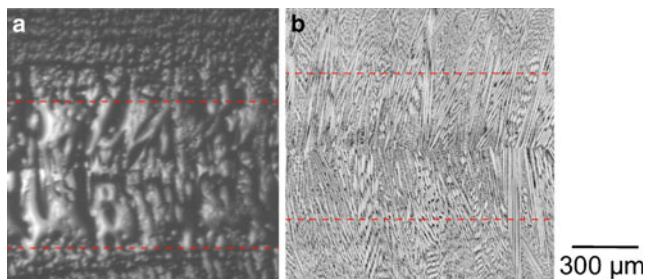
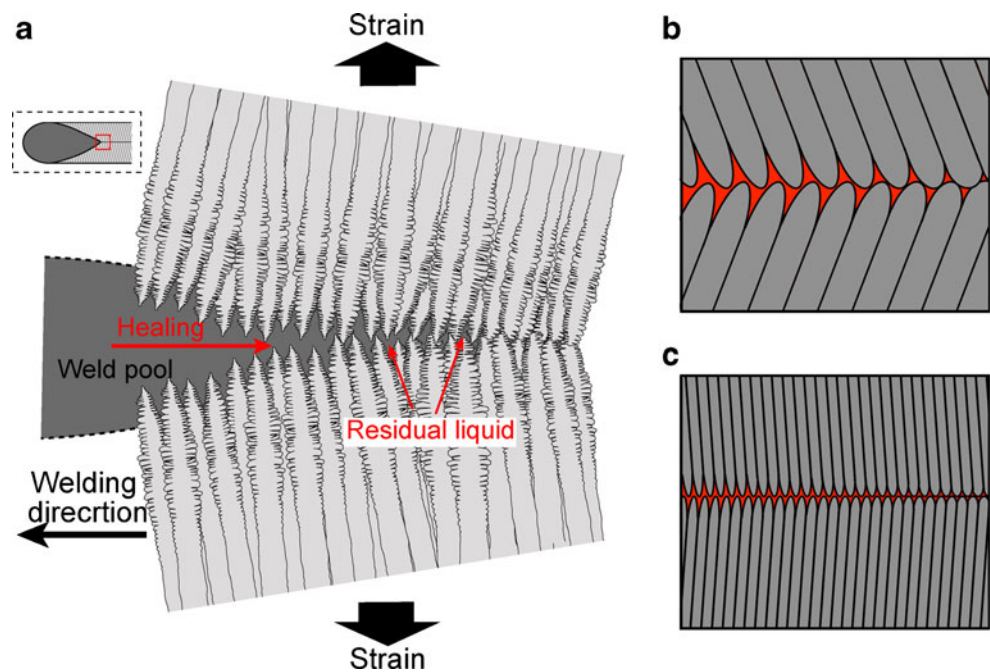


Fig. 9 Comparison of image between in-situ observation and microstructure (welding speed: 1.6 m/min) **a** in-situ observation **b** microstructure

attributed to the deterioration in strength perpendicular to the welding direction; therefore, the critical strain value for crack initiation during the U-type hot cracking test decreases with increase in welding speed.

To help explain the phenomenon of the residual liquid distribution quantitatively, Fig. 10 shows schematic illustrations of the residual liquid at the rear of the molten pool during laser welding at high welding speeds. Columnar dendrites grow perpendicularly to the welding direction and bridge with columnar dendrites growing from the opposite side at the center of the weld bead (Fig. 10a). When the high temperature position is compared with that at the bridging point, the liquid between the dendrites is sufficient to heal incipient cracks since the position connects with the molten pool, if the strain is loaded at the rear of the molten pool. At low temperature, the liquid between the dendrites continues to remain at the interface between the dendrite tips (weld bead center). The residual liquid solidifies (dendrite arm growth). In addition, it can be assumed that the distribution of residual liquid depends on microstructure. As shown in Fig. 6, when the welding speed is fast (1.6 m/min), the interface between the dendrite tips at the center of the weld bead becomes smooth, because the microstructure consists of very fine columnar dendrites

Fig. 10 Schematic illustrations of distribution of residual liquid during laser welding **a** Morphology of residual liquid **b** High welding speed **c** Low welding speed



that grow perpendicularly to the welding direction. Therefore, the liquid remains as a thin continuous liquid film at the interface between the dendrite tip (Fig. 10b). On the other hand, when the welding speed is slow (0.4 m/min), the columnar dendrites become coarse and grow in an inclined direction to the welding direction. This microstructure leads to the formation of a rough interface; thus, the residual liquid exists as segmentalized (droplet) morphology (Fig. 10c).

The distribution of residual liquid depends on the microstructure. The residual liquid at the interface between the dendrite tips (weld bead center) causes the generation of a solidification crack under high welding speed conditions. It is well known that the residual liquid distribution affects the solidification cracking susceptibility. If the liquid exists as a film, the continuous interface of the dendrite tips forms and makes the material susceptible to solidification cracking. Therefore, the transition of distribution morphology of the residual liquid from droplet to film with increasing welding speed induces the susceptibility to solidification cracking.

4 Summary

The solidification cracking susceptibility of Type 310S stainless steels under high welding speed conditions (laser welding) was investigated as a function of welding speed. In-situ observations by high-speed video camera enabled quantitative, high accuracy measurement of the critical strain for solidification cracking. The temperature histories during high-speed laser welding could be measured

using an optical fiber radiation thermometer. The critical strain for solidification cracking decreased with increasing welding speed. This could be caused by the distribution morphology of the residual liquid at the dendrite tip interface (weld bead center). The distribution in residual liquid depended on the microstructure at the rear of the molten pool. The transition in residual morphology from droplet to film with increasing welding speed can be attributed to the susceptibility in solidification cracking.

Open Access This article is distributed under the terms of the Creative Commons Attribution License which permits any use, distribution, and reproduction in any medium, provided the original author(s) and the source are credited.

References

1. Dupont J, Lippold J, Kiser S (2009) *Welding metallurgy and weldability of nickel-base alloys*. John Wiley & Sons. Inc, Hoboken, New Jersey
2. Kou S (2003) *Welding metallurgy*. John Wiley & Sons. Inc, Hoboken, New Jersey
3. Borland JC (1960) Generalized theory of super-solidus cracking in welds. *Br Weld J* 7:508–512
4. Matsuda F, Nakagawa H, Sorada K (1982) Dynamic observation of solidification and solidification cracking during welding with optical microscope. *Trans JWRI* 11(2):67–77
5. David SA, White CL, Kujanpaa VP (1986) Formation of hot cracks in austenitic stainless steel welds- solidification cracking. *Weld J* 65(8):203–212
6. Saida K (2010) Weldability of stainless steels. *J Jpn Weld Soc* 79(6):582–592

7. J Lippold (1994) Solidification behavior and cracking susceptibility of pulsed-laser welds in austenitic stainless steels. *Weld J* 73 (6):129s–140s
8. Osuki T, Hirata H, Ogawa K (2007) Numerical analysis of solidification process of austenitic stainless steel weld metal with dependence of welding velocity* -Study of solidification structure on austenitic stainless steel weld metal. *Q J Jpn Weld Soc* 25 (1):140–148
9. Wen P, Yamamoto M, Senda Y, Tamura T, Shinozaki K (2010) Study on solidification cracking of laser dissimilar welded joints by using in-situ observation and numerical simulation. *Weld World* 54(9–10):R257–R266
10. Shinozaki K, Yamamoto M, Tamura T, Wen P (2008) Development of evaluation method for solidification cracking susceptibility of Inconel/SUS347 dissimilar laser weld metal by in-situ observation. *Mater Sci Forum* 580–582:49–52